Biosensors and Bioelectronics 151 (2020) 111983

Contents lists available at ScienceDirect

Biosensors and Bioelectronics

journal homepage: http://www.elsevier.com/locate/bios

High peroxidase-like activity realized by facile synthesis of FeS_2 nanoparticles for sensitive colorimetric detection of H_2O_2 and glutathione

Chan Song *, Wei Ding, Weiwen Zhao, Haibo Liu, Jie Wang, Yuewei Yao, Cheng Yao **

School of Chemistry and Molecular Engineering, Nanjing Tech University, Nanjing, 211816, China

ARTICLE INFO

Keywords:
FeS_2 NPs
Peroxidase-like activity
Mimics
Colorimetric
Biosensor

ABSTRACT

In the last decades, enzyme mimics have been regarded as strong substitutes to natural enzymes. The construction of biosensors based on these enzyme mimics with competitive catalytic activity and substrate specificity has attracted a lot of research interest. Herein, for the first time, we investigated the capability of nanoscale FeS_2 to serve as enzyme mimics. Then, a facile and effective biosensor is fabricated based on its intrinsic peroxidase-like catalytic activity. In the presence of H_2O_2, FeS_2 nanoparticles (NPs) possess high peroxidase-like activity to 3,3′,5,5′-tetramethylbenzidine (TMB) oxidation, which can be ascribed to the generation of hydroxyl radicals (·OH) from the H_2O_2 decomposition catalyzed by FeS_2 NPs. As for TMB, the resulting Michaelis−Menten constant (K_m) value of FeS_2 NPs is found to be about 12 times lower than that of natural horseradish peroxidase (HRP), highlighting the superiority of FeS_2 NPs. Based on these intriguing observations, a reliable colorimetric method is then developed for detection of H_2O_2 and glutathione (GSH) by a simple mix-and-detect strategy. The detection limits of H_2O_2 and GSH are as low as 0.91 μM and 0.15 μM (3σ/slope), respectively. Moreover, FeS_2 NPs can also catalyse the photoluminescence (PL) substrate terephthalic acid (TA) under the assistance of H_2O_2. This work remarkably extends the utilization of FeS_2 NPs in the construction of colorimetric and PL biosensors in the fields of biosensing, environmental monitoring, and medical diagnosis.

1. Introduction

As a class of efficient biological catalysts involved in almost all reactions *in vivo*, natural enzymes with high catalytic activity and high substrate specificity have been successfully employed in various fields (Wolfenden and Snider, 2001; Filizola and Loew, 2000). However, the high cost of preparation and rigorous storage conditions severely hinder their further practical applications. These issues of natural enzymes have triggered intensive research interest in the development of novel enzyme mimics. Early in 2007, ferromagnetic nanoparticles (Fe_3O_4 NPs) were proven to possess an intrinsic peroxidase-like activity by Yan's group (Gao et al., 2007). This observation indicated that Fe_3O_4 NPs could catalyse the oxidation of some organic substrates in the presence of H_2O_2, just like horseradish peroxidase (HRP) or some other natural peroxidases. Since then, novel nanomaterials have been considered as competitive alternatives of nature enzymes, due to their numerous merits, such as high stability and cost-effectiveness (Wu et al., 2019a; Liu et al., 2019a,b; Liu and Liu, 2017; Lin et al. 2014a,b,c). Plenty of nanomaterials, such as noble metals, metal oxides, carbon-based materials, and metal organic frameworks (MOFs), have been extensively explored to serve as the enzyme mimics in the design of biosensors in recent years (Li et al., 2019; Jin et al., 2019; Hu et al., 2017; Han et al., 2017; Lin et al. 2014a,b,c; Zhang et al., 2019; Shi et al., 2011; Chen et al., 2018a,b). However, the catalytic efficiency of these artificial enzymes is still far inferior to that of natural enzymes (Zhou et al., 2017). Thus, the development of enzyme mimics with highly activity and highly affinity to substrates is still urgent and vital.

Recently, several kinds of transition metal chalcogenides (TMCs) are found to possess the intrinsic peroxidase-like catalytic activity. For instance, the two-dimensional transition metal dichalcogenides (TMDs), involving VS_2, MoS_2, and WS_2 nanosheets (NSs), can serve as enzyme mimics in the sensing systems for the detection of H_2O_2 and glucose (Huang et al., 2018; Xia et al., 2019; Lin et al. 2014a,b,c). Besides, the hollow copper sulfide nanocubes (h-CuS NCs), prepared by Wang's group very recently, also show excellent peroxidase-like activity (Zhu et al., 2019). The presence of copper endows the proposed h-CuS NCs with the characteristics of Fenton's reagents, resulting in better mimetic performance. The remarkable catalysis characteristics of TMCs,

* Corresponding author.
** Corresponding author.
E-mail addresses: songchan@njtech.edu.cn (C. Song), yaocheng@njtech.edu.cn (C. Yao).

https://doi.org/10.1016/j.bios.2019.111983
Received 3 August 2019; Received in revised form 24 November 2019; Accepted 20 December 2019
Available online 23 December 2019
0956-5663/

especially TMDs, can be mainly attributed to their excellent physico-chemical properties (Sajedi-Moghaddam et al., 2017; Butler et al., 2013; Chen et al., 2015; Zhou et al., 2012). Based on those observations, we believe that the iron-based TMCs (FeS_x) might also hold a great potential to be the appropriate candidates for mimicking peroxidases.

As a representative of iron-based TMCs, FeS_2 has been widely investigated in various fields due to its suitable band gap ($E_g = 0.95$ eV) and extraordinary absorption coefficient ($\alpha > 10^5$ cm^{-1} for hv >1.3 eV) (Liu et al., 2017; Xu et al., 2018; Zhang et al., 2018a,b; Douglas et al., 2015; Hu et al., 2018). However, the investigation of nanoscale FeS_2 as enzyme mimics and the subsequent utilization in biosensing is still in its infancy. Herein, FeS_2 NPs are firstly synthesized *via* a facile one-step sulfidation of Fe_3O_4 NPs with sulfur powder (Scheme 1a). These as-prepared FeS_2 NPs are demonstrated to possess high peroxidase-like enzyme activity, which is prerequisite for peroxidase mimics. Furthermore, a label-free colorimetric method is constructed to realize the visual detection of H_2O_2 and glutathione (GSH) by one-pot biosensing (Scheme 1b). Importantly, the FeS_2 NPs-based sensing system could be also utilized in the assay of GSH in real samples. We believe that this work would provide a new paradigm for broadening the application of FeS_2 nanomaterials in the biosensing field.

2. Experimental section

2.1. Materials and methods

3,3′,5,5′-tetramethylbenzidine (TMB), 2,2′-azino-bis(3-ethylbenzothiazoline-6-sulfonic acid) (ABTS), bull serum albumin (BSA), protamine, glucose oxidase (GOx), lysozyme, and glucose were provided by Sangon Biotech. Co. Ltd. (Shanghai, China). GSH (reduced form) was obtained from Aladdin (Shanghai, China). $FeCl_3{\cdot}6H_2O$, terephthalic acid (TA), and H_2O_2 were purchased from Sinopharm Chemical Reagent Co., Ltd. (Shanghai, China). 5,5-dimethyl-1-pyrroline N-oxide (DMPO) and human serum sample were provided by Energy Chemical Reagent Co., Ltd. (Shanghai, China) and Solarbio Science & Technology Co., Ltd. (Beijing, China), respectively. Human serum experiments were performed in compliance with the protocol approved by the Ethics Committee at Nanjing Tech University (No. 2019-1). All the chemicals were obtained from commercial sources and used as received.

Powder X-ray diffraction spectra (PXRD) were formed on a Rigaku D/Max-2500 diffractometer equipped with a Cu K_α radiation source. Transmission electron microscopy (TEM) images were obtained from Talos L120C (FEI, USA). Analysis of the X-ray photoelectron spectra (XPS) was performed on a Thermo ESCALAB 250 spectrometer. The ζ-potential was measured by a Nanosizer ZS90 (Malvern). Fluorescence measurements were carried out by a F97XP spectrofluorimeter with the excitation and emission slit widths of 10 nm. UV-vis absorption spectra were acquired by a Persee TU-1900 double beam UV-vis spectrophotometer.

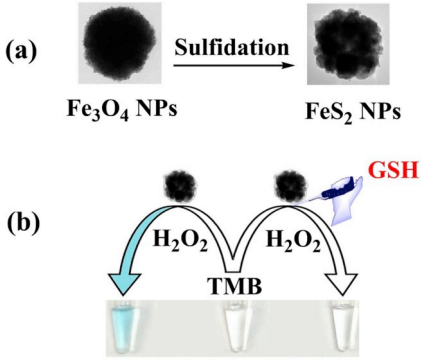

Scheme 1. Schematic illustration of the formation of FeS_2 NPs (a) and colorimetric detection of H_2O_2 and GSH based on FeS_2 NPs as the sensing platforms (b).

2.2. Synthesis of FeS_2 NPs

FeS_2 NPs were synthesized by the sulfidation of Fe_3O_4 NPs. Firstly, Fe_3O_4 NPs were prepared according to previous literature (Wang et al., 2018a,b). In a typical process, $FeCl_3{\cdot}6H_2O$ (2.432 g, 9 mmol) and trisdium citrate (0.774 g, 3 mmol) were dissolved in ethylene glycol (60 mL) by stirring for 1 h. After that, sodium acetate (3.6 g, 43.9 mmol) was added to the mixture, which was continuously stirred for another 1 h. After ultrasonication for 0.5 h, the solution was sealed in a 100 mL Teflon-lined autoclave and heated at 200 °C for 10 h. After cooling to room temperature, the black Fe_3O_4 NPs were obtained by centrifugation (9000 rpm, 10 min) and washing with distilled water/ethanol (1:1, v/v) for three times. Subsequently, the mixture containing Fe_3O_4 NPs and excess sulfur powder was loaded in the quartz boat covered by aluminum foil and heated at 400 °C for 5 h with a ramp of 2 °C min^{-1} under the atmosphere of argon to get the final product of FeS_2 NPs.

2.3. Colorimetric detection of H_2O_2 and GSH

Varied concentrations of H_2O_2 or different amounts of GSH with 0.08 mM H_2O_2 were mixed with 10 mM HAc-NaAc buffer solution (pH 4.0) containing 0.2 mM TMB and 0.3 mg L^{-1} FeS_2 NPs. The total volume of mixture was 100 μL and the amounts of above mentioned chemicals were final concentrations. Then, the mixture was incubated at 45 °C for 1 h. Finally, the UV-vis spectra of the obtained samples were recorded and the absorbance intensity at 652 nm was used for quantitative detection of H_2O_2 or GSH. All experiments were performed in triplicate.

2.4. In vitro cytotoxicity

HeLa cells were incubated in RPMI 1640 medium supplemented with 10% fetal bovine serum and 1% penicillin-streptomycin at 37 °C in a humidified atmosphere of 5% CO_2. To determine the cytotoxicity, HeLa cells were seeded in 96-well plates for 24 h to allow cell attachment and stabilization. Then, the cells were treated with different concentrations of FeS_2 NPs ranged from 0 to 5 mg L^{-1} (final concentration). After incubating for 24 h, 150 μL MTT solution (5 g L^{-1}) was added and incubated for another 4 h. Subsequently, the medium was replaced with 150 μL DMSO. Finally, the absorbance at 570 nm of each well was determined and cell viability was calculated by the formula of Cell viability = Abs(sample)/Abs(control) ×100%.

3. Results and discussion

3.1. Synthesis and characterization of FeS_2 NPs

The synthesis of FeS_2 NPs was accomplished by the straightforward sulfidation of Fe_3O_4 NPs. The XRD pattern and transmission electron microscopy (TEM) image confirm that Fe_3O_4 NPs with a diameter of about 170 nm have been successfully prepared (Figs. 1a and S1). After sulfidation, the precursor Fe_3O_4 NPs were completely converted into FeS_2 NPs (JCPDS card No. 71-1680), confirmed by the XRD analysis (Fig. 1a). TEM image shows that FeS_2 NPs have successfully inherited the uniform morphology of Fe_3O_4 NPs with diameters of about 200 nm (Fig. 1b). The slight increased diameter compared to that of Fe_3O_4 NPs can be ascribed to the injection of sulfur element. The chemical state and composition shown in XPS survey spectrum further demonstrated the successful synthesis of FeS_2 NPs (Fig. S2). In order to evaluate the feasibility of employing FeS_2 NPs as enzyme mimics, the cytotoxicity of FeS_2 NPs was evaluated by using HeLa cells. Fig. 1c shows that the viability of HeLa cells could remain above 96.8% even with the presence of 5 mg L^{-1} FeS_2 NPs. The low cytotoxicity of FeS_2 NPs would pave the way for their subsequent application in the field of biosensing.

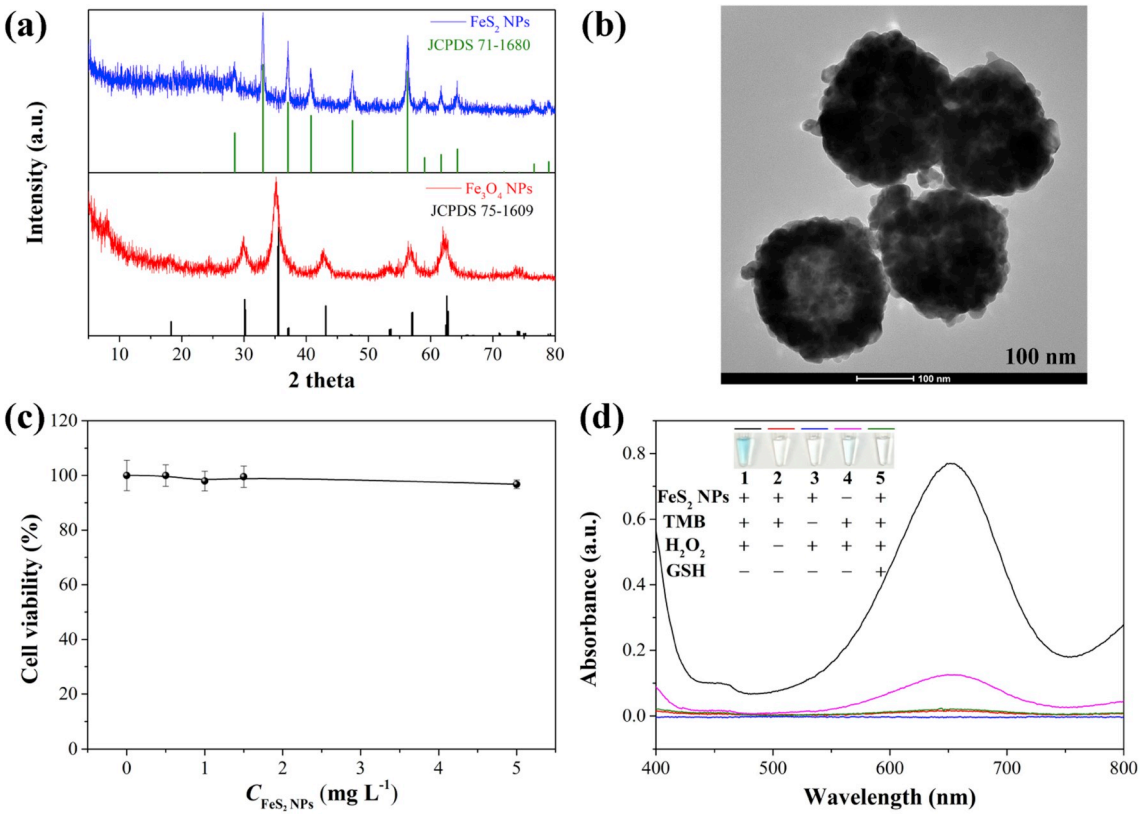

Fig. 1. (a) PXRD patterns of as-synthesized Fe_3O_4 NPs and FeS_2 NPs. (b) Typical TEM image of FeS_2 NPs. (c) The cell viability of Hela cells in the presence of different amounts of FeS_2 NPs (0, 0.5, 1, 1.5 and 5 mg L^{-1}). (d) UV-vis absorption spectra of reaction system with different reagents: (1) FeS_2 NPs + TMB + H_2O_2, (2) FeS_2 NPs + TMB, (3) FeS_2 NPs + H_2O_2, (4) TMB + H_2O_2, (5) FeS_2 NPs + TMB + H_2O_2 + GSH. Inset: ingredients and photographs of corresponding samples. The symbol '+' indicates the presence of corresponding component, while symbol '-' represents the absence. [FeS_2 NPs] = 0.3 mg L^{-1}, [TMB] = 0.2 mM, [H_2O_2] = 0.08 mM, [GSH] = 50 μM.

3.2. Peroxidase-like activity of FeS_2 NPs and H_2O_2 sensing

The peroxidase-like activity of FeS_2 NPs was first explored by the catalytic oxidation of colorimetric substrate 3,3′,5,5′-tetramethylbenzidine (TMB) in the presence of H_2O_2. With the addition of FeS_2 NPs, the color for the mixture of TMB and H_2O_2 (Fig. 1d, lane 4) turned deep-blue (Fig. 1d, lane 1) and a maximum absorption peak at 652 nm was observed (Fig. 1d, black curve), indicating the generation of the blue product oxTMB. Meanwhile, no significant color and absorbance intensity change of FeS_2 NPs with TMB or H_2O_2 only could be found (lane 2 and red curve, lane 3 and blue curve). The UV-vis absorption spectra shown in Fig. S3 demonstrated that FeS_2 NPs had no absorbance in the wavelength range 400–800 nm. These results implied that the presence of FeS_2 NPs could effectively promote the oxidation reaction. Similarly, another typical colorimetric substrate, 2,2′-azino-bis(3-ethylbenzothiazoline-6-sulfonic acid) (ABTS) can also be catalyzed by FeS_2 NPs in the presence of H_2O_2 (Fig. S4). Namely, the prominent intrinsic peroxidase-like activity of FeS_2 NPs guarantees their utilization as peroxidase enzyme mimics.

Fig. 2a showed the gradually deepened color of solution containing TMB and H_2O_2 along with the increased concentration of FeS_2 NPs. The stronger absorbance signal was stemmed from the higher activity of FeS_2 NPs. Thus, the intrinsic peroxidase-like activity of FeS_2 NPs was the catalyst dose-dependent. It is noteworthy that the dosage of 0.45 mg L^{-1} for FeS_2 NPs could deliver the absorbance intensity ~1 a.u. for TMB−H_2O_2 solution, demonstrating the high peroxidase-like activity of FeS_2 NPs. Subsequently, the optimal experimental conditions on the activity of FeS_2 NPs were investigated. The acidity of reaction solution and temperature had a great influence on the enzyme activity of FeS_2 NPs. The reaction pH higher than 5.0 would accelerate the decomposition of H_2O_2, resulting in the decrease of its oxidation activity (Roy et al., 2012a). Not surprisingly, FeS_2 NPs also exhibited the highest catalytic activity at pH 4.0 (Fig. 2b), just like many other previously reported mimics (Wu et al., 2019b; Su et al., 2012). Similar to other colorimetric substrates such as *N*,*N*-diethyl-*p*-phenylenediamine sulfate (DPD), TMB could be slowly oxidized by H_2O_2 at pH 4.0 (Yang et al., 2019). As shown in Fig. 2c, the oxidation reaction optimal temperature of FeS_2 NPs was about 45 °C like Fe_3O_4 NPs. This may be attributed to similar bond strength between Fe and O or S, resulting in the generation of a maximum amount of iron ions (Roy et al., 2012b). Besides, the absorbance signal reached a plateau after 60 min (Fig. 2d). Further experiment had been carried out to verify the excellent stability of FeS_2 NPs, as the enzyme activity of FeS_2 NPs was still fully maintained even after soaking in water for 40 days (Fig. S5). These remarkable features endowed FeS_2 NPs with great potential for the construction of novel biosensors.

At the optimized conditions, the absorbance intensity of FeS_2 NPs-based catalytic system at 652 nm increased remarkably with the addition of H_2O_2 in the low concentration range and achieved a plateau with 400 μM H_2O_2 (Fig. 2e). Fig. 2f showed that H_2O_2 concentration between 2 μM and 80 μM gave a good linear correlation with the enhancement of absorbance signal ($\Delta A = 0.0082 + 0.0095\ C_{H2O2}$, $R_1^2 = 0.9989$, $\Delta A = A - A_0$, where A and A_0 are the absorbance of FeS_2 NPs and TMB with and without H_2O_2, respectively). The detection limit was as low as 0.91 μM (3σ/slope). In addition, another excellent linear relationship was observed in the H_2O_2 concentration ranged from 80 μM to 200 μM ($\Delta A = 0.4734 + 0.0036\ C_{H2O2}$, $R_2^2 = 0.9987$) with the detection limit of 2.34 μM (3σ/slope). This phenomenon was also noted in the previous works (He et al., 2018; Zheng et al., 2018; Yao et al., 2019). The difference in linear slope between the two H_2O_2 concentration ranges may be

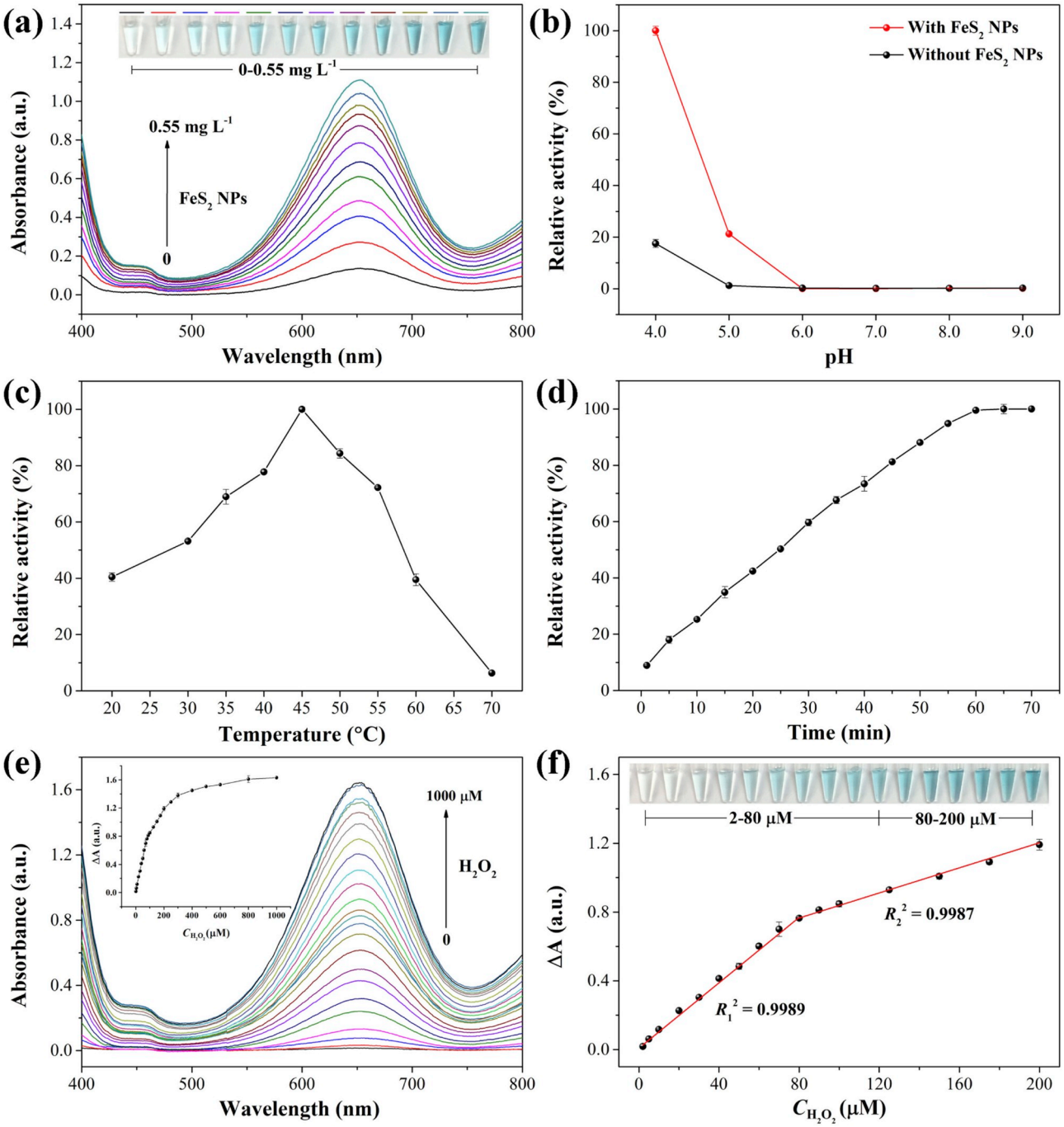

Fig. 2. (a) UV-vis absorption spectra of TMB (0.2 mM) and H_2O_2 (0.08 mM) with different amounts of FeS_2 NPs (0, 0.05, 0.1, 0.15, 0.2, 0.25, 0.3, 0.35, 0.4, 0.45, 0.5, and 0.55 mg L^{-1}). Inset: photographs of corresponding samples. (b) pH-, (c) temperature- and (d) time-dependent activity of FeS_2 NPs (0.3 mg L^{-1}) in the presence of TMB (0.2 mM) and H_2O_2 (0.08 mM). (e) UV-vis absorption curves of FeS_2 NPs (0.3 mg L^{-1}) and TMB (0.2 mM) with different amounts of H_2O_2 at pH 4.0. Inset: the absorbance enhancement ($\Delta A = A - A_0$) with increasing concentration of H_2O_2. A and A_0 are the absorbance intensity of FeS_2 NPs and TMB with and without H_2O_2, respectively. (f) The linear calibration plots for the detection of H_2O_2. Inset: photographs of corresponding samples.

ascribed to the diverse reaction states of nanozymes with H_2O_2 (Du et al., 2019; Peng et al., 2019; Mi et al., 2018). Namely, at lower concentration, the added H_2O_2 could interact more effectively with FeS_2 NPs. At the same time, the color variation of the reaction samples can be obviously observed (Fig. 2f, inset), offering the visual assay of H_2O_2 by naked eyes. Therefore, a facile colorimetric method for H_2O_2 detection could be developed on the basis of peroxidase-like property of FeS_2 NPs by a simple mix-and-detect approach. Notably, the broader linear range and lower detection limit of FeS_2 NPs for the colorimetric detection of H_2O_2 were superior to some previously reported nanomaterial-based sensing platforms (Table S1).

3.3. Catalytic mechanism of FeS_2 NPs

As shown in Fig. 2a and 2e, except for the enzyme activity of mimics, the concentration of H_2O_2 also played an important role in the catalytic oxidation of TMB by FeS_2 NPs. In order to investigate the catalytic mechanism of FeS_2 NPs, the electron paramagnetic resonance (EPR) spectroscopy was firstly employed to trap the presence of hydroxyl radicals (·OH) with 5,5-dimethyl-1-pyrroline-*N*-oxide (DMPO) (Wang

et al., 2017; Jiao et al., 2019). In comparison with the sample including DMPO and H_2O_2, the addition of 5 mg L^{-1} FeS_2 NPs gave strong characteristic peaks of the typical DMPO-·OH adducts (Fig. 3a), indicating the generation of ·OH in the reaction system (Zhang et al., 2018a,b). According to previous reports (Ai et al., 2013), the catalytic process of FeS_2 NPs might be finished by two steps. First, ·OH was released due to the interaction of FeS_2 NPs with H_2O_2. Subsequently, TMB was oxidized by ·OH, leading to the formation of oxTMB. Predictably, higher dosage of FeS_2 NPs would give rise to more ·OH and stronger peak intensity. The red curve shown in Fig. 3a just validated this hypothesis, in which 20 mg L^{-1} FeS_2 NPs brought higher activity of mimics and dramatically increased peak intensity.

The catalytic mechanism of FeS_2 NPs was further excavated by a photoluminescence (PL) method, in which TA was employed as a PL probe. As shown in Fig. 3b (black curve) and S6, both TA and FeS_2 NPs exhibited no PL intensity in the emission wavelength from 350 nm to 600 nm at pH 4.0. However, TA can react with ·OH to generate a PL product 2-hydroxy terephthalic acid (Chen et al., 2018a,b; Deng et al., 2019). Apparently, the PL intensity at 425 nm gradually increased with the rising dosage of FeS_2 NPs at pH 4.0 (Fig. 3b), implying the increased

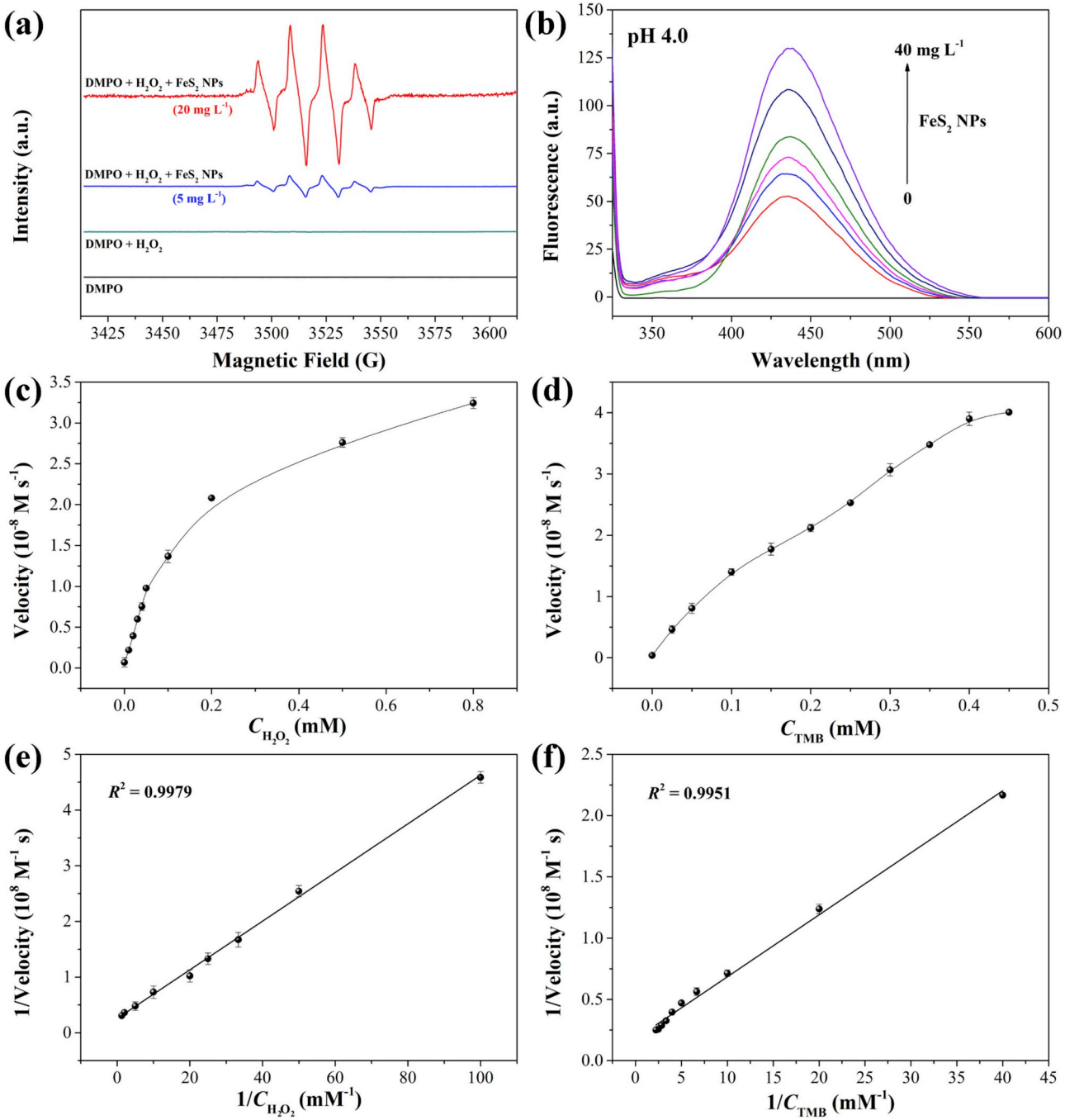

Fig. 3. (a) EPR spectra of different reaction samples with DMPO (100 mM) as the spin trap. [H_2O_2] = 100 mM. (b) Fluorescence spectra of TA (0.625 mM) and H_2O_2 (50 mM) with different concentration of FeS_2 NPs (0, 2.5, 5, 10, 20, 30 and 40 mg L^{-1}) under pH 4.0. The excitation wavelength was set to 314 nm. Steady-state kinetic analysis by utilizing the Michaelis-Menten model (c and d) and Lineweaver–Burk double-reciprocal model (e and f) for FeS_2 NPs (0.3 mg L^{-1}) at pH 4.0. (c) Reaction velocity plots with a fixed TMB concentration (0.2 mM) and various H_2O_2 amounts. (d) Reaction velocity plots with a fixed H_2O_2 concentration (0.2 mM) and various TMB amounts. (e) and (f) Double reciprocal plots of FeS_2 NPs with the concentration of one substrate (H_2O_2 or TMB) varied.

content of ·OH. These phenomena demonstrated that the peroxidase-like activity of FeS_2 NPs was originated from their catalytic decomposition of H_2O_2 to release ·OH (Wang et al., 2018a,b). Besides, fluorescence substrate TA could also be effectively catalyzed by FeS_2 NPs even under neutral solution (Fig. S7), indicating the utilization of FeS_2 NPs as sensing platform for fluorescence detection of biomolecules such as H_2O_2, glucose and GSH.

Finally, the steady-state kinetic assay was studied by varying the concentration of TMB or H_2O_2 in the FeS_2 NPs-based catalytic system. As shown in Fig. 3c and 3d, the oxidation reaction catalyzed by FeS_2 NPs exhibited the typical Michaelis−Menten curves for both substrates. Additionally, double reciprocal Michaelis−Menten curves were fitted to the Lineweaver−Burk equation $1/v = (K_m/V_{max})\times(1/[S]) + 1/V_{max}$ (Fig. 3e and 3f), in which v is initial velocity, K_m is Michaelis−Menten constant, V_{max} is the maximum reaction velocity and $[S]$ is the concentration of the substrate. The K_m and V_{max} were then calculated according to the Lineweaver−Burk equation. As shown in Table S2, the K_m value of FeS_2 NPs with H_2O_2 (0.30 mM) is much lower than that of HRP (3.7 mM) and some previously reported nanomaterial-based peroxidase mimics. The lower K_m value indicates a higher affinity of mimics to the substrates. Besides, when taking TMB as the substrate, FeS_2 NPs also possess superior affinity to those reported ones except FeS NPs, whose K_m value with TMB was as low as 0.008 mM (Maji et al., 2012). Notably, the K_m value of FeS_2 NPs using TMB as the substrate is 0.17 mM, which is much lower than that of HRP (0.43 mM). In order to further examine the mechanism about the strong binding ability of FeS_2 NPs to TMB, the zeta-potential measurement was carried out. As shown in Fig. S8, the pristine FeS_2 NPs gave a strong negative charge (−4.88 mV) under pH 4.0. However, the addition of TMB significantly reduced the negative charge (−0.10 mV). The more positive feature stemmed from TMB could be assigned to the fact that the nonoxidized TMB (pK_a ~4.2) could carry partial positive charge in pH 4.0 because of the presence of two amino groups. In other words, the strong affinity of FeS_2 NPs to TMB may derive from the strong electrostatic interaction between them at pH 4.0.

3.4. GSH detection based on FeS_2 NPs as the sensing platform

As the most abundant tripeptide thiol in eukaryotic cells, GSH plays an important role in defensing against toxins and free radicals. The abnormal of GSH levels can reflect the symptom of some diseases such as caners, liver injury, and acquired immune deficiency syndrome (Meister and Anderson, 1983; Perry et al., 1993; Fruehauf and Meyskens, 2007). Thus, the exploration of simple and reliable technologies for GSH detection has gained growing interest in disease diagnosis and biomedical methodologies. As an antioxidant, GSH can be used as a reductant to facilitate the reduction of the oxTMB (Liu et al., 2019a,b; Feng et al., 2017; Shamsipur et al., 2014). As shown in Fig. 1d, the substrate TMB could be catalyzed by FeS_2 NPs with H_2O_2, producing a blue-colored oxTMB with high absorbance signal at 652 nm (lane 1, black curve). After the addition of GSH, a colorless solution was obtained (Fig. 1d, lane 5) and no absorption could be detected (Fig. 1d, green curve). Based on this inhibition effect of GSH toward the TMB oxidation by FeS_2 NPs in the presence of H_2O_2, a facile colorimetric method was then constructed for the detection of GSH by a facile one-step approach (Scheme 1b).

Under the optimum reaction condition, the sensitivity of the proposed GSH sensing system was investigated by introducing different concentration of targets. With the increasing dosage of GSH, the absorbance signal at 652 nm decreased gradually and the reduction of corresponding absorbance intensity ($\Delta A = A_0 - A$, where A_0 and A are the absorbance of the sensing system with and without GSH) increased systematically (Fig. 4a). The absorbance value reached a plateau when the GSH dose is up to 40 μM. Accordingly, as shown in Fig. 3b, the change of absorbance exhibited a good linear relationship with the concentration of GSH ranging from 0.2 μM to 35 μM ($R^2 = 0.9967$). The detection limit for GSH assay could reach 0.15 μM (3σ/slope), which is much superior to some previous reports (Table S3). These results indicated that the presented approach in this study was sensitive for GSH evaluation. Moreover, the color variation of the corresponding samples containing different amounts of GSH could be clearly discriminated on visual observation (Fig. 4b, inset photos). Therefore, the FeS_2 NPs-based sensing platform can offer a simple method for the visual assay of GSH by naked eyes.

The specificity is equally vital to an excellent biosensor. Thus, the selectivity of the GSH determination based on the peroxidase-like activity of FeS_2 NPs has been investigated by screening its response to biological molecules and ions. First, the interference effect of amino acids on this method was checked. As shown in Fig. 5, the presence of histidine (His), arginine (Arg), lysine (Lys), methionine (Met), aspartate (Asp), glutamine (Glu), and asparagine (Asp) cannot inhibit the oxidation of TMB catalyzed by FeS_2 NPs with the aid of H_2O_2, as reflecting by the deep blue color of corresponding samples. As expected, the presence of cysteine (Cys) delivered a colorless solution, just like the consequence of GSH addition (Fig. 5, inset photos). As an effective component of GSH, the Cys possessed a reasonable inhibition on the oxidation of TMB (Ma et al., 2018). However, as the content of GSH in real biological system is much higher than that of Cys, the selectivity of this proposed sensing system to GSH was quite acceptable (Chi et al., 2018; Yao et al., 2017).

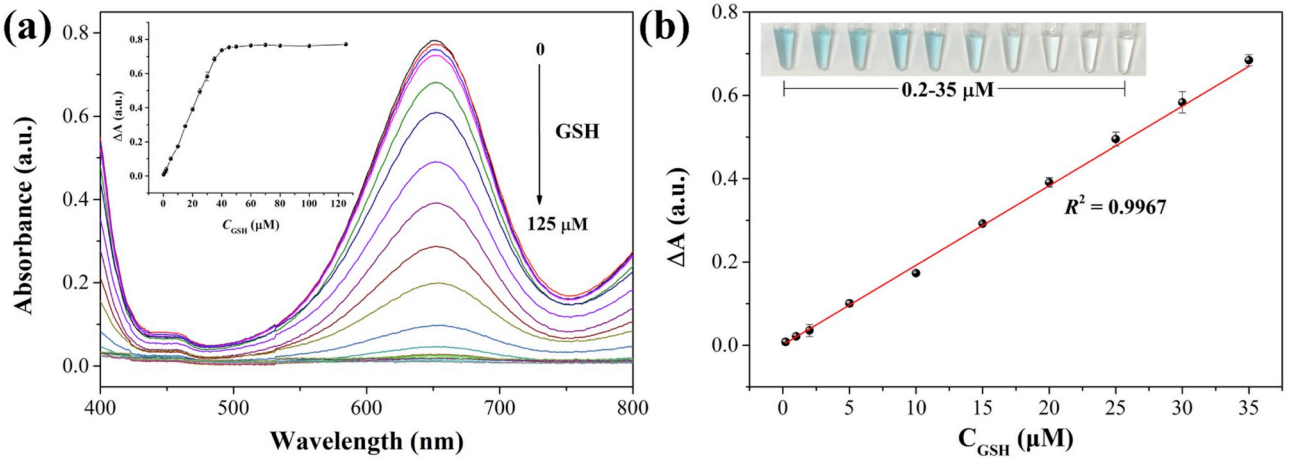

Fig. 4. (a) UV-vis absorption curves of FeS_2 NPs (0.3 mg L^{-1}) with TMB (0.2 mM) and H_2O_2 (0.08 mM) in the presence of different concentration of GSH at pH 4.0. Inset: the absorbance change ($\Delta A = A_0 - A$) with increasing concentration of GSH. A and A_0 are the absorbance of reaction system with and without GSH, respectively. (b) The linear calibration plot for GSH sensing. Inset: the photographs of corresponding samples.

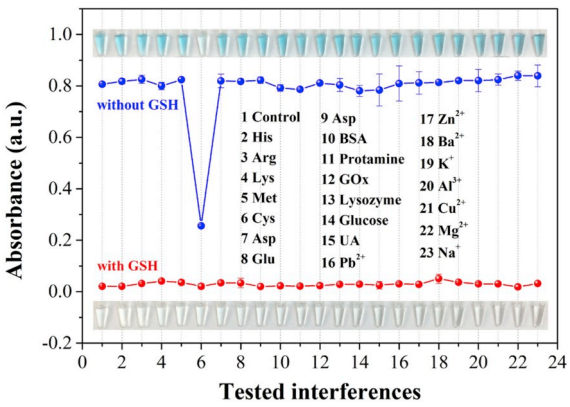

Fig. 5. The specificity and anti-interference analysis of the GSH detection. Concentrations of GOx, BSA and protamine are 10 mg L^{-1} and amounts of GSH and other common interfering species are 50 μM. Inset: the photographs of corresponding reaction samples. [FeS_2 NPs] = 0.3 mg L^{-1}, [TMB] = 0.2 mM, [H_2O_2] = 0.08 mM.

Besides, no obvious change of absorbance intensity could be detected before and after the addition of some biological molecules, including bull serum albumin (BSA), protamine, glucose oxidase (GOx), lysozyme, glucose and uric acid (UA). Meanwhile, common cations (*e.g.* Pb^{2+}, Zn^{2+}, Ba^{2+}, K^{+}, Al^{3+}, Cu^{2+}, Mg^{2+}, Na^{+}) also have little effect on the absorbance intensity. These phenomena validated the excellent specificity of FeS_2 NPs-based sensing platform.

Furthermore, the anti-interference of this method was tested by adding the abovementioned substances to the samples containing target GSH, respectively. Fig. 5 showed that the coexistence of GSH and interferences also exhibited the strong inhibition ability to peroxidase-like activity of FeS_2 NPs, obtaining the colorless solutions and low absorbance intensities. However, the presence of GSH would reasonably mask the effect of Cys, since 50 μM GSH has significantly reduced the absorbance signal. These results demonstrated that this sensing system have a high anti-interference ability to GSH detection.

The potential feasibility of this colorimetric method in real biological environment was evaluated by adding three concentrations of GSH (5 μM, 15 μM, and 25 μM) to 1% and 3% human serum sample, respectively. The absorbance value at 652 nm was recorded and the reduction of absorbance intensity (ΔA) was then used to achieve the recoveries from the calibration graph. As shown in Tables S4 and S5, the recovery values were varied between 98.4% and 103.4%. These satisfactory recoveries demonstrated the potential employment of this proposed FeS_2 NPs-based sensing system in the assay of GSH in the real samples.

4. Conclusion

In summary, uniform FeS_2 NPs with excellent peroxidase-like activity were prepared by a facile approach. Further investigations have demonstrated that the proposed FeS_2 NPs can effectively catalyze the oxidation of colorimetric substrates such as TMB, ABTS, and TA in the presence of H_2O_2. This fascinating feature of FeS_2 NPs is stemmed from their capability to effective catalytic decomposition of H_2O_2 into ·OH. A facile colorimetric method for H_2O_2 detection is then fabricated by employing FeS_2 NPs-based enzyme mimics as the sensing platform. Moreover, based on the inhibition effect of GSH on the peroxidase-like activity of FeS_2 NPs, the GSH sensing system with high sensitivity and specificity is also developed. This investigation provides an open opportunity for the construction of versatile nanomaterials-based biosensor in the fields of biosensing, environmental monitoring, and medical diagnosis.

Author contribution

Chan Song conceived and designed the experiments; Wei Ding, Weiwen Zhao, Haibo Liu and Jie Wang performed the experiments; Chan Song, Yuewei Yao, and Cheng Yao analysed the data; Chan Song and Wei Ding wrote the paper.

Declaration of competing interest

The authors declare that they have no known competing financial interests or personal relationships that could have appeared to influence the work reported in this paper.

CRediT authorship contribution statement

Chan Song: Conceptualization, Data curation, Funding acquisition, Methodology, Supervision, Validation, Writing - original draft, Writing - review & editing. **Wei Ding:** Investigation, Writing - original draft. **Weiwen Zhao:** Investigation. **Haibo Liu:** Investigation. **Jie Wang:** Investigation. **Yuewei Yao:** Investigation. **Cheng Yao:** Resources, Supervision, Validation.

Acknowledgement

This work was supported by the National Natural Science Foundation of China (21801132) and Postgraduate Research & Practice Innovation Program of Jiangsu Province (KYCX18_1062). We also thank Prof. De-Ming Kong (Nankai University) for his help in discussion on mechanism.

Appendix A. Supplementary data

Supplementary data to this article can be found online at https://doi.org/10.1016/j.bios.2019.111983.

References

Ai, L., Li, L., Zhang, C., Fu, J., Jiang, J., 2013. Chem. Eur J. 19, 15105–15108.
Butler, S.Z., Hollen, S.M., Cao, L., Cui, Y., Gupta, J.A., Gutierrez, H.R., Heinz, T.F., Hong, S.S., Huang, J., Ismach, A.F., Johnston-Halperin, E., Kuno, M., Plashnitsa, V. V., Robinson, R.D., Ruoff, R.S., Salahuddin, S., Shan, J., Shi, L., Spencer, M.G., Terrones, M., Windl, W., Goldberger, J.E., 2013. ACS Nano 7, 2898–2926.
Chen, Y., Tan, C., Zhang, H., Wang, L., 2015. Chem. Soc. Rev. 44, 2681–2701.
Chen, W.H., Vazquez-Gonzalez, M., Kozell, A., Cecconello, A., Willner, I., 2018. Small 14, 1703149.
Chen, T., Zou, H., Wu, X., Liu, C., Situ, B., Zheng, L., Yang, G., 2018. ACS Appl. Mater. Interfaces 10, 12453–12462.
Chi, M., Chen, S., Zhong, M., Wang, C., Lu, X., 2018. Chem. Commun. 54, 5827–5830.
Deng, H.H., Luo, B.Y., He, S.B., Chen, R.T., Lin, Z., Peng, H.P., Xia, X.H., Chen, W., 2019. Anal. Chem. 91, 4039–4046.
Douglas, A., Carter, R., Oakes, L., Share, K., Cohn, A.P., Pint, C.L., 2015. ACS Nano 9, 11156–11165.
Du, Q., Hu, X., Zhang, X., Cao, H., Huang, Y., 2019. Anal. Methods 11, 3446–3451.
Feng, J., Huang, P., Shi, S., Deng, K.Y., Wu, F.Y., 2017. Anal. Chim. Acta 967, 64–69.
Filizola, M., Loew, G.H., 2000. J. Am. Chem. Soc. 122, 18–25.
Fruehauf, J.P., Meyskens Jr., F.L., 2007. Clin. Cancer Res. 13, 789–794.
Gao, L., Zhuang, J., Nie, L., Zhang, J., Zhang, Y., Gu, N., Wang, T., Feng, J., Yang, D., Perrett, S., Yan, X., 2007. Nat. Nanotechnol. 2, 577–583.
Han, L., Shi, J., Liu, A., 2017. Sens. Actuators B 252, 919–926.
He, Y., Qi, F., Zhang, W., Zhang, X., Niu, X., Pan, J., 2018. Anal. Chim. Acta 1021, 113–120.
Hu, Y., Cheng, H., Zhao, X., Wu, J., Muhammad, F., Lin, S., He, J., Zhou, L., Zhang, C., Deng, Y., Wang, P., Zhou, Z., Nie, S., Wei, H., 2017. ACS Nano 11, 5558–5566.
Hu, R., Zhao, H., Zhang, J., Liang, Q., Wang, Y., Guo, B., Dangol, R., Zheng, Y., Yan, Q., Zhu, J., 2018. Nanoscale 11, 178–184.
Huang, L., Zhu, W., Zhang, W., Chen, K., Wang, J., Wang, R., Yang, Q., Hu, N., Suo, Y., Wang, J., 2018. Microchim. Acta 185, 1–8.
Jiao, L., Xu, W., Yan, H., Wu, Y., Liu, C., Du, D., Lin, Y., Zhu, C., 2019. Anal. Chem. 91, 11994–11999.
Jin, S., Wu, C., Ye, Z., Ying, Y., 2019. Sens. Actuators B 283, 18–34.
Li, S., Shang, L., Xu, B., Wang, S., Gu, K., Wu, Q., Sun, Y., Zhang, Q., Yang, H., Zhang, F., Gu, L., Zhang, T., Liu, H., 2019. Angew. Chem. Int. Ed. 58, 12624–12631.
Lin, Y., Ren, J., Qu, X., 2014. Acc. Chem. Res. 47, 1097–1105.
Lin, Y., Ren, J., Qu, X., 2014. Adv. Mater. 26, 4200–4217.
Lin, T., Zhong, L., Song, Z., Guo, L., Wu, H., Guo, Q., Chen, Y., Fu, F., Chen, G., 2014. Biosens. Bioelectron. 62, 302–307.

Liu, B., Liu, J., 2017. Nano Res. 10, 1125–1148.
Liu, Z., Lu, T., Song, T., Yu, X.-Y., Lou, X.W., Paik, U., 2017. Energy Environ. Sci. 10, 1576–1580.
Liu, X., Huang, D., Lai, C., Qin, L., Zeng, G., Xu, P., Li, B., Yi, H., Zhang, M., 2019. Small 15, 1900133.
Liu, Y., Zhou, M., Cao, W., Wang, X., Wang, Q., Li, S., Wei, H., 2019. Anal. Chem. 91, 8170–8175.
Ma, H., Li, X., Liu, X., Deng, M., Wang, X., Iqbal, A., Liu, W., Qin, W., 2018. Sens. Actuators B 255, 1687–1693.
Maji, S.K., Dutta, A.K., Biswas, P., Srivastava, D.N., Paul, P., Mondal, A., Adhikary, B., 2012. Appl. Catal. A Gen. 419-420, 170–177.
Meister, A., Anderson, M.E., 1983. Annu. Rev. Biochem. 52, 711–760.
Mi, Y., Lei, X., Han, H., Liang, J., Liu, L., 2018. Anal. Methods 10, 4170–4177.
Peng, C., Xing, H., Fan, X., Xue, Y., Li, J., Wang, E., 2019. Anal. Chem. 91, 5762–5767.
Perry, R.R., Mazetta, J., Levin, M., Barranco, S.C., 1993. Cancer 72, 783–787.
Roy, P., Lin, Z.H., Liang, C.T., Chang, H.T., 2012. Chem. Commun. 48, 4079–4081.
Sajedi-Moghaddam, A., Saievar-Iranizad, E., Pumera, M., 2017. Nanoscale 9, 8052–8065.
Shamsipur, M., Safavi, A., Mohammadpour, Z., 2014. Sens. Actuators B 199, 463–469.
Shi, W., Wang, Q., Long, Y., Cheng, Z., Chen, S., Zheng, H., Huang, Y., 2011. Chem. Commun. 47, 6695–6697.
Su, L., Feng, J., Zhou, X., Ren, C., Li, H., Chen, X., 2012. Anal. Chem. 84, 5753–5758.
Wang, Y.M., Liu, J.W., Adkins, G.B., Shen, W., Trinh, M.P., Duan, L.Y., Jiang, J.H., Zhong, W., 2017. Anal. Chem. 89, 12327–12333.
Wang, Q., Luo, W., Chen, X., Fan, J., Jiang, W., Wang, L., Jiang, W., Zhang, W.X., Yang, J., 2018. Chemistry 24, 15663–15668.
Wang, C., Gao, J., Cao, Y., Tan, H., 2018. Anal. Chim. Acta 1004, 74–81.
Wolfenden, R., Snider, M.J., 2001. Acc. Chem. Res. 34, 938–945.
Wu, J., Wang, X., Wang, Q., Lou, Z., Li, S., Zhu, Y., Qin, L., Wei, H., 2019. Chem. Soc. Rev. 48, 1004–1076.
Xia, W., Zhang, P., Fu, W., Hu, L., Wang, Y., 2019. Chem. Commun. 55, 2039–2042.
Xu, X., Meng, Z., Zhu, X., Zhang, S., Han, W.-Q., 2018. J. Power Sources 380, 12–17.
Yang, F., Jiang, G., Yan, F., Chang, Q., 2019. Microchim. Acta 186, 417.
Yao, C., Wang, J., Zheng, A., Wu, L., Zhang, X., Liu, X., 2017. Sens. Actuators B 252, 30–36.
Yao, J., Wu, T., Sun, Y., Ma, Z., Liu, M., Zhang, Y., Yao, S., 2019. Talanta 195, 265–271.
Zhang, M.-Y., Cui, Z.-H., Jiang, H., 2018. J. Mater. Chem. 6, 6606–6616.
Zhang, Q., Chen, S., Wang, H., Yu, H., 2018. ACS Appl. Mater. Interfaces 10, 8666–8675.
Zhang, P., Sun, D., Cho, A., Weon, S., Lee, S., Lee, J., Han, J.W., Kim, D.P., Choi, W., 2019. Nat. Commun. 10, 940.
Zheng, H.Q., Liu, C.Y., Zeng, X.Y., Chen, J., Lu, J., Lin, R.G., Cao, R., Lin, Z.J., Su, J.W., 2018. Inorg. Chem. 57, 9096–9104.
Zhou, Y., Wang, Z., Yang, P., Zu, X., Yang, L., Sun, X., Gao, F., 2012. ACS Nano 6, 9727–9736.
Zhou, Y., Liu, B., Yang, R., Liu, J., 2017. Bioconjug. Chem. 28, 2903–2909.
Zhu, J., Peng, X., Nie, W., Wang, Y., Gao, J., Wen, W., Selvaraj, J.N., Zhang, X., Wang, S., 2019. Biosens. Bioelectron. 141, 111450.